Check for updates

ADVANCED MATERIALS
www.advmat.de

Pathology-Driven Design of a Biomimetic Ferromagnetic Nanomedicine for Dual-Mode Treatment of Ulcerative Colitis and Colitis-Associated Colorectal Cancer

Shengsheng Liu, Baoyi Li, Qiang Yang, Menghang Zu, Haiting Xu, Bozhao Li, Pu Li, Jun Zhang, Liqi Li, Zhenhua Zhu, Xiang Peng, Xiao Yang, Mohammad-Ali Shahbazi, Xiaoxiao Shi, Rui L. Reis, Subhas C. Kundu, Guangjun Nie,* and Bo Xiao**

The pathological features of ulcerative colitis (UC) involve systemic abnormalities, including immune dysregulation, iron deficiency, and microbiota imbalance, and these alterations contribute to an increased risk of colitis-associated colorectal cancer (CAC). Current therapeutic strategies remain insufficient to address these pathological features and restore physiological homeostasis. Here, a dual-duty nanomedicine (MAC@EGCG-Fe_3O_4), engineered with an inflammation-homing M2-type macrophage membrane "shell" is rationally designed and developed, which encapsulates silk fibroin nanocages loading with epigallocatechin gallate (EGCG) and ferromagnetic nanoparticles (Fe_3O_4). Upon intraperitoneal injection and exposure to an alternating magnetic field (AMF), the nanomedicine selectively accumulated in inflamed lesions, enabling site-specific therapeutic effects. Controlled AMF irradiation provided localized mild hyperthermia and reductive EGCG for UC treatment or hyperpyrexia and oxidative EGCG for treating CAC. Moreover, this therapeutic strategy reprogrammed colonic immune responses, restored mucosal integrity, alleviated iron deficiency, and modulated microbiota and its metabolites. The study highlights the therapeutic potential of a single pathology-driven nanomedicine against both UC and CAC through AMF manipulation.

1. Introduction

Ulcerative colitis (UC) is a chronic, incurable gastrointestinal disorder with a rising global incidence.[1] This disease is characterized by recurrent colonic inflammation,[2,3] excessive oxidative stress,[4] disrupted epithelial barrier,[5] and iron-deficiency anemia.[6] A key pathological hallmark of UC is the local recruitment and polarization of macrophages into the pro-inflammatory M1 phenotype,[7] which exacerbates inflammation, disrupts gut microbiota homeostasis, and contributes to metabolic dysfunction, ultimately increasing the risk of colitis-associated colorectal cancer (CAC).[8] Current therapeutic strategies, including 5-aminosalicylic acid (5-ASA),[9] dexamethasone sodium phosphate (DSP),[10] and biological agents,[11] primarily aim to suppress inflammation. However, their clinical utility is often limited by suboptimal efficacy, severe side effects, and an inability to reduce CAC incidence.[12–14]

S. Liu, B. Li, M. Zu, B. Xiao
Department of Pharmacy
Personalized Drug Research and Therapy Key Laboratory of Sichuan Province
Sichuan Academy of Medical Sciences & Sichuan Provincial People's Hospital
School of Medicine
University of Electronic Science and Technology of China
Chengdu 610054, China
E-mail: bxiao@uestc.edu.cn

S. Liu, Q. Yang, H. Xu, X. Yang, X. Shi
State Key Laboratory of Resource Insects
College of Sericulture
Textile, and Biomass Sciences, Southwest University
Chongqing 400715, China
E-mail: xxshi7@swu.edu.cn

The ORCID identification number(s) for the author(s) of this article can be found under https://doi.org/10.1002/adma.202514413

B. Li, G. Nie
CAS Key Laboratory for Biomedical Effects of Nanomaterials & Nanosafety
CAS Center for Excellence in Nanoscience
National Center for Nanoscience and Technology
Beijing 100190, China
E-mail: niegj@nanoctr.cn

B. Li
Institutes of Biomedical Sciences
Inner Mongolia University
Hohhot 010070, China

P. Li
Department of Clinical Laboratory
The Second Affiliated Hospital of Chongqing Medical University
Chongqing 400010, China

J. Zhang
HIFU Tumor Treatment Center
The Second Affiliated Hospital of Chongqing Medical University
Chongqing 400010, China

DOI: 10.1002/adma.202514413

 © 2026 Wiley-VCH GmbH

15214095, 2026, 6, Downloaded from https://advanced.onlinelibrary.wiley.com/doi/10.1002/adma.202514413 by Universidade Do Minho, Wiley Online Library on [21/04/2026]. See the Terms and Conditions (https://onlinelibrary.wiley.com/terms-and-conditions) on Wiley Online Library for rules of use; OA articles are governed by the applicable Creative Commons License

These challenges underscore the urgent need for rationally designed nanomedicines capable of addressing the complex pathological features of colonic diseases and restoring physiological homeostasis.

Exogenous thermal therapy holds great promise as a multi-role therapeutic strategy for treating both UC and CAC by controlling operating temperatures.[15] Mild thermotherapy consistently reprograms macrophages, attenuates inflammation, and restores barriers,[16] whereas local hyperpyrexia effectively ablates tumor cells and triggers antitumor immunity.[17] Interestingly, as a natural catechin, epigallocatechin gallate (EGCG) exhibits anti-inflammatory and anti-cancer properties with a favorable safety profile.[18,19] Importantly, previous literature has reported conflicting findings regarding EGCG's role in ROS scavenging versus generation.[20,21] Therefore, we hypothesize that EGCG may dynamically coordinate ROS production and scavenging under certain conditions. Alternating magnetic field (AMF) is an optimal signal for manipulating ferromagnetic particles to treat various diseases (e.g., glioblastoma multiforme, esophageal cancer, and pancreatic cancer) due to its unparalleled tissue-penetrating capability, maneuverability, and exceptional biosafety.[22–24] The off-target distribution hampers the efficiency of therapeutic agents on account of their inadequate accumulation in the inflammatory and tumor lesions.[25] Accumulating evidence substantiates the potential of M2-type macrophage membranes (MACs) for targeted drug delivery into the inflammatory tissues (e.g., atherosclerotic plaque, pancreatitis, and osteoarthritis),[26] which is ascribed to their facile generation, strong inflammatory tropism, and ability to absorb inflammatory cytokines.[27]

Here, we proposed a single biomimetic nanomedicine, inflammation-homing MAC-coated EGCG/Fe_3O_4-loaded nanoparticles (MAC@EGCG-Fe_3O_4 NPs), for specific and effective treatment of both UC and CAC (**Scheme 1**). After intraperitoneal (*ip*) injection, MAC@EGCG-Fe_3O_4 homed to the inflammation-associated sites and accumulated in the colitis mucosa and colitis-associated colorectal tumors. Subsequently, it was internalized by the target cells and achieved efficient lysosome escape and controlled drug release upon exposure to AMF. By adjusting the AMF output, MAC@EGCG-Fe_3O_4 plus mild magnetothermia (MMT: AMF irradiation, 2 min) demonstrated a favorable anti-colitis effect by mitigating inflammation, scavenging reactive species, and promoting M1-to-M2 macrophage repolarization. Conversely, combined with hypermagnetothermia (HMT: AMF irradiation, 3 min) and αPD-L1, it ablated orthotopic and distant colorectal tumors by activating innate and adaptive immunities and eliciting long-term antitumor immune memory. Significantly, the treatment of MAC@EGCG-Fe_3O_4 plus AMF irradiation could also replenish iron levels, restoring intestinal barrier integrity and reshaping microbial metabolites. Eventually, our findings demonstrate that the AMF-controlled MAC@EGCG-Fe_3O_4 notably ameliorates the disease symptoms of inflamed and tumoral colons, making it a promising platform for targeted treatment of colitis and its related cancerous disease.

2. Result

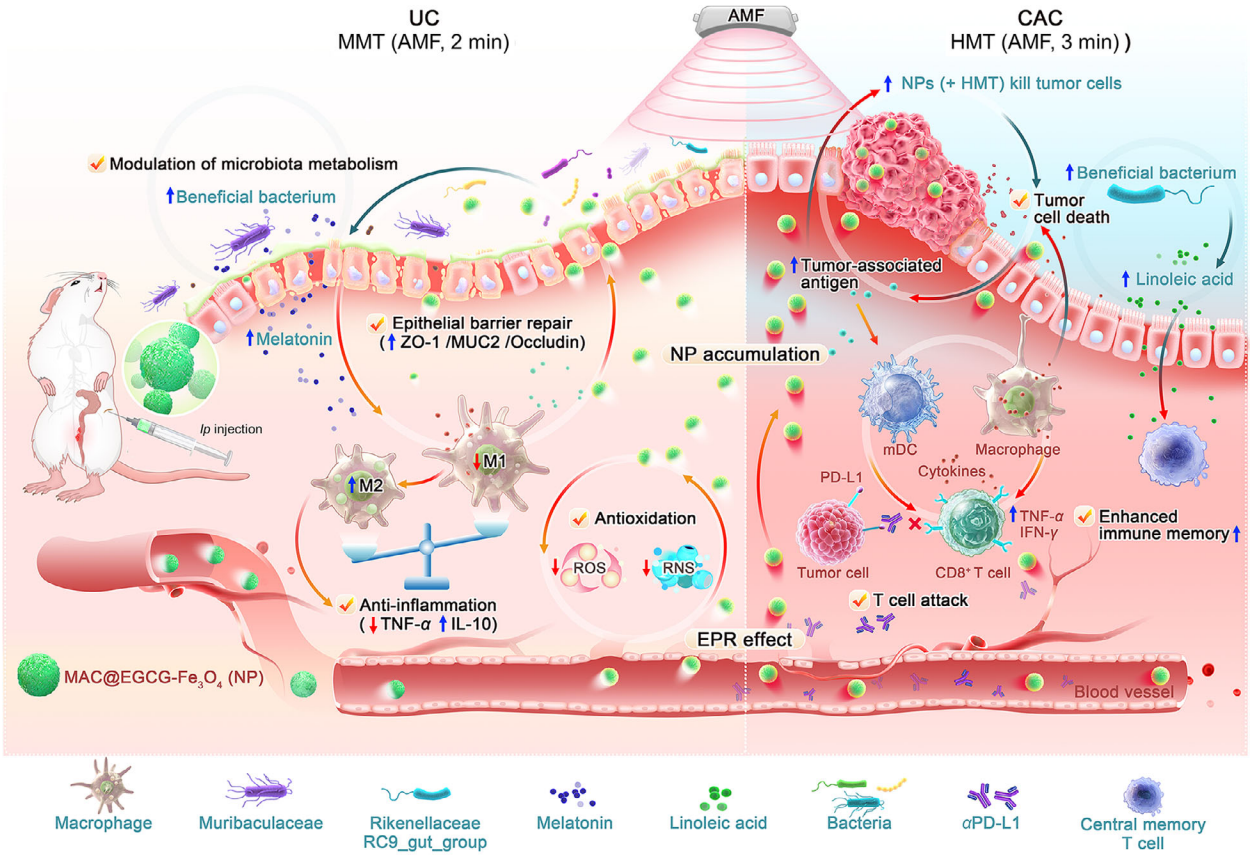
2.1. Human Colon Tissue Analysis and UC Therapeutic Effect of M2-Type Macrophages

Macrophages play a central role in the progression of colonic diseases.[28] Accordingly, we benchmarked their phenotypes in the colon tissues of human patients with UC and CAC. A positive correlation was observed between disease severity and the abundance of pro-inflammatory M1-type macrophages using a confocal laser scanning microscope (CLSM) (**Figure 1A–C**). We hypothesized that prioritising scavenging inflammation and repolarizing anti-inflammatory macrophages might represent a promising strategy for managing colitis and its associated colorectal cancer. Therefore, we initially constructed an inflammation-scavenging nanoreactor consisting of a regenerated silk fibroin (RSF) nanocage encapsulating EGCG. The EGCG-loaded RSF-based NPs (EGCG-NPs) were spherical and monodispersed, possessing an average size of 162.5 nm and a negative potential of –20.4 mV (Figure 1D; Figure S1, Supporting Information). When exposed to macrophages, EGCG-NPs drove the repolarization of macrophages toward the anti-inflammatory M2 phenotype for up to 72 h (Figure 1E,F; Figure S2, Supporting Information). In contrast, treatment with blank NPs or free EGCG resulted in a slightly increased CD206 expression only at the 24- and 48-h intervals, followed by a marked decline in expression levels.

Peritoneal macrophages were polarized toward M1-phenotype when stimulated with lipopolysaccharide (LPS) and induced to M2-phenotype in response to EGCG-NPs or IL-4 (Figure 1G). It was observed that in comparison to the LPS-treated group, both EGCG-NPs and M2-type peritoneal macrophages (especially the latter) demonstrated significant anti-inflammatory capabilities, as manifested by a 10.8% and 43.5% reduction in pro-inflammatory TNF-α level, along with a 13.9-fold and 25.6-fold increase in the secretion of anti-inflammatory IL-10 (Figure 1H,I). The inflammatory state of colitis mucosa is often accompanied by a substantial buildup of reactive species, including reactive

L. Li
Department of General Surgery
The Second Affiliated Hospital of Army Medical University (Xinqiao Hospital)
Chongqing 400037, China
Z. Zhu
Department of Gastroenterology
The First Affiliated Hospital of Nanchang University
Nanchang 330006, China
X. Peng
Department of Gastroenterology
The Sixth Affiliated Hospital of Sun Yat-Sen University
Guangzhou 510655, China
M.-A. Shahbazi
Department of Biomaterials and Biomedical Technology
The Personalized Medicine Research Institute (PRECISION)
University Medical Center Groningen
University of Groningen
Antonius Deusinglaan 1, Groningen, AV 9713, Netherlands
R. L. Reis, S. C. Kundu
3Bs Research Group, I3Bs — Research Institute on Biomaterials, Biodegradables and Biomimetics, Headquarters of the European Institute of Excellence on Tissue Engineering and Regenerative Medicine
University of Minho
AvePark, Barco, Guimaraes 4805-017, Portugal

 © 2026 Wiley-VCH GmbH



Scheme 1. Schematic illustration of MAC@EGCG-Fe_3O_4 for the treatment of UC and CAC. Fe_3O_4-NPs and EGCG were co-loaded into RSF-based NPs, and the obtained EGCG-Fe_3O_4 NPs were further coated with M2-type MAC to enhance their inflammation-targeting capability. Mice were intraperitoneally injected with MAC@EGCG-Fe_3O_4 and treated with AMF irradiation. Upon entering the bloodstream, the MAC-@EGCG-Fe_3O_4 was selectively recruited to the colitis mucosa and colitis-associated colorectal tumor. When combined with MMT (AMF, 2 min), MAC@EGCG-Fe_3O_4 effectively eliminated ROS and RNS in the colitis mucosa and facilitated polarization of M1-type macrophages toward the M2-type. This process led to a reduction in TNF-α level, an increase in IL-10 expression, and an up-regulation of tight junction proteins (ZO-1/MUC2/Occludin), thereby restoring the colonic epithelial barrier, down-regulating inflammatory reactions, and modulating intestinal microbiota and metabolites. When combined with HMT (AMF, 3 min), MAC@EGCG-Fe_3O_4 effectively penetrated and accumulated in the deep colorectal tumor tissues, caused tumor cell apoptosis, and induced the release of tumor-associated antigens to recruit T cells. The further combination with αPD-L1 could stimulate T-cell activation and trigger the secretion of chemokines and cytokines for enhanced tumor cell death, immune cell recruitment, and regulation of intestinal microbial metabolism.

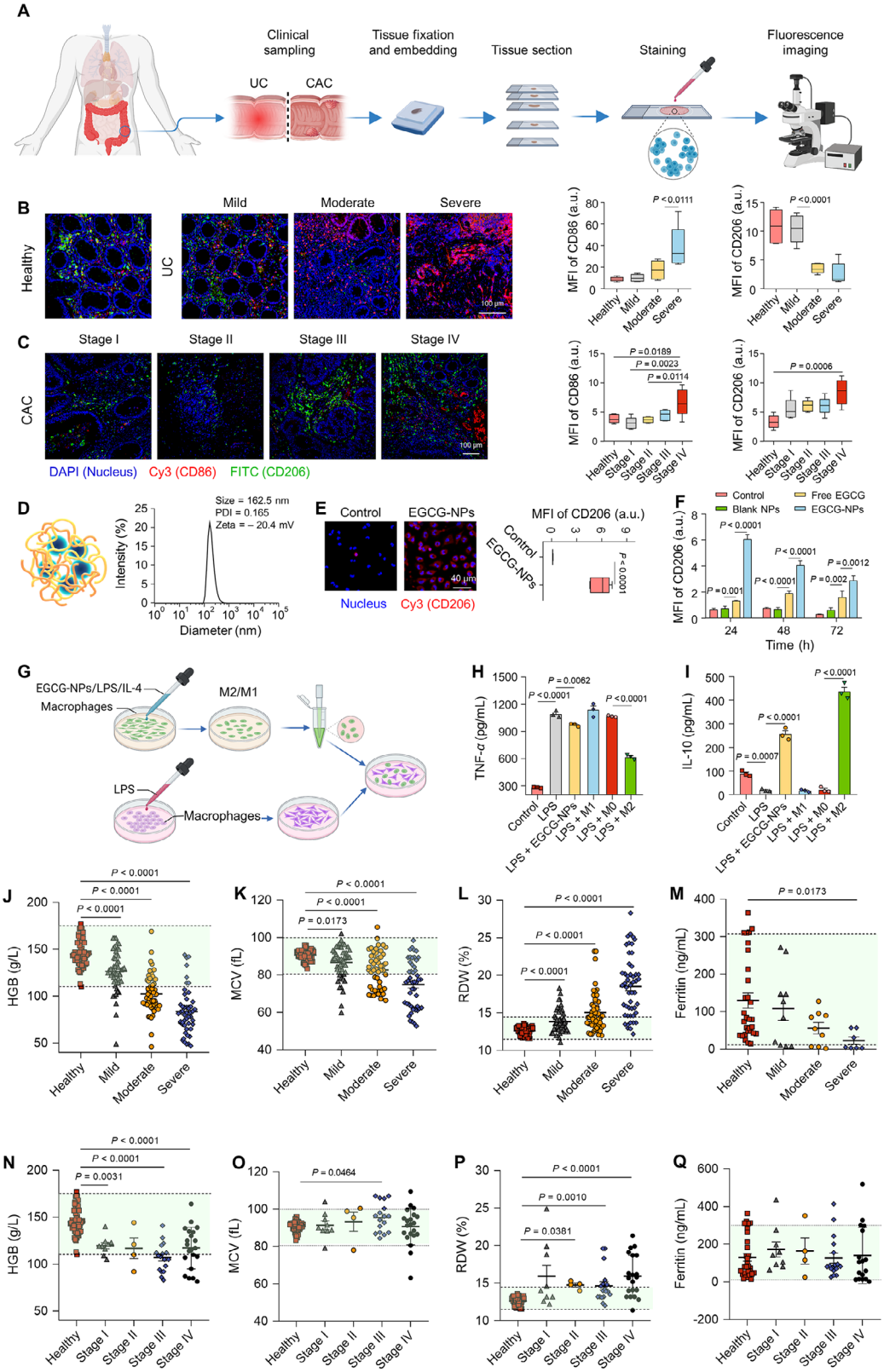
oxygen/nitrogen species (ROS/RNS). LPS-induced productions of ROS and RNS were effectively obliterated after treating EGCG-NPs and M2-type macrophages (Figure S3A–D, Supporting Information), suggesting their strong antioxidative capacity.

The accumulation of NPs in the diseased tissues is essential for exerting their in vivo therapeutic effect.[29] In dextran sulfate sodium (DSS)-induced UC mice, Cy7-modified EGCG-NPs showed higher enrichment in the inflamed colons via *ip* injection compared with the intravenous (*iv*) route (Figure S3E,G, Supporting Information). Regrettably, there was an unexpected hepatic accumulation of EGCG-NPs. We evaluated the in vivo distribution characteristics of different macrophage types to determine the optimal alternative for inflammation. Interestingly, intraperitoneally injected M2-type macrophages preferentially localized in the colitis mucosa rather than the healthy colon and other organs (Figure S3F,H, Supporting Information), which might be attributable to their chemotactic effect.[30]

The inflamed colon-targeting capacity and anti-inflammatory effect of M2-type macrophages inspired us to investigate their impact on UC development (Figure S4A, Supporting Information). After discontinuing DSS, all mice showed weight restoration (Figure S4B, Supporting Information), without any discernible damage to the major organs (Figure S4G, Supporting Information). Compared with the DSS control group, which exhibited a colon length of 6.1 ± 0.3 cm, *ip* injection of M1-type macrophages induced a much shorter colon length (5.5 ± 0.2 cm) (Figure S4C, Supporting Information), suggesting that this type of macrophage could exacerbate inflammatory conditions. We intuitively observed a substantial presence of M2-type (CD206) macrophages and scarce M1-type (CD86) macrophages in the colon tissues from the M2-type macrophage-treated mice (Figure S4D–F, Supporting Information), supporting that M2-type macrophages could drive the polarization of activated M1-type macrophages in the colitis tissues to exert an anti-inflammatory effect. Strikingly, the treatment of M2-type macrophages effectively alleviated the DSS-induced symptoms, including colon shortening, increased spleen index, elevated myeloperoxidase (MPO) activity (Figure S4C,H,I, Supporting

© 2026 Wiley-VCH GmbH

15214095, 2026, 6, Downloaded from https://advanced.onlinelibrary.wiley.com/doi/10.1002/adma.202514413 by Universidade Do Minho, Wiley Online Library on [21/04/2026]. See the Terms and Conditions (https://onlinelibrary.wiley.com/terms-and-conditions) on Wiley Online Library for rules of use; OA articles are governed by the applicable Creative Commons License



© 2026 Wiley-VCH GmbH

15214095, 2026, 6, Downloaded from https://advanced.onlinelibrary.wiley.com/doi/10.1002/adma.202514413 by Universidade Do Minho, Wiley Online Library on [21/04/2026]. See the Terms and Conditions (https://onlinelibrary.wiley.com/terms-and-conditions) on Wiley Online Library for rules of use; OA articles are governed by the applicable Creative Commons License

Information), and increased pro-inflammatory TNF-α and IL-6 concentrations, as well as decreased IL-10 levels, in comparison with the clinical DSP and other treatment groups (Figure S4J,L,M, Supporting Information). It is universally acknowledged that controlling macrophage polarization possesses the expertise for ameliorating symptoms associated with colitis.[31] Histological analyses showed that M2-type macrophages effectively repaired the damaged colonic epithelial barrier and reduced the infiltration of inflammatory cells (Figure S4K,N,O, Supporting Information), with no obvious abnormalities observed in the principal organs (Figure S5, Supporting Information).

2.2. Rational Design, Fabrication, and Characterization of MAC@EGCG-Fe_3O_4

The "pathology-driven design strategy" constitutes a pivotal paradigm in exploring therapeutic systems. In addition to examining the phenotypes of macrophages in the colon tissues from human UC/CAC patients, we further analyzed their blood parameters. Figure 1J–Q presented the patients' abnormal indices and low ferritin levels compared to healthy volunteers. This symptom, termed iron-deficiency anemia, would exacerbate the disease state and impede the therapeutic efficacy of medications.[32] To address this issue, FDA-approved Fe_3O_4 NPs were incorporated into EGCG-NPs, enabling iron supplementation and utilizing their heat effect induced by AMF for mitigating colitis and ablating colorectal tumors, while assisting in anti-tumor therapy of EGCG. We validated the differential effects of EGCG, in combination with either MMT or HMT, on CT-26 and RAW 264.7 cells. Under MMT conditions, EGCG displayed potent ROS-scavenging properties, whereas under HMT conditions, it exerted ROS-generating capacity (Figure S6A–D, Supporting Information). This discrepancy can be attributed to the formation of a catechol structure by EGCG under MMT, which could scavenge ROS by donating hydrogen atoms (Figure S7, Supporting Information). Notably, under HMT, EGCG switched to quinone derivatives that could compromise cellular antioxidant capacity, elevating ROS levels and inducing cytotoxicity (Figure S8, Supporting Information). We did find that HMT-assisted EGCG treatment significantly decreased the viabilities of CT-26 cells relative to MMT-treated EGCG (Figure S6E–G, Supporting Information).[33] In addition, HPLC-MS analysis of EGCG-treated CT-26 cell lysates yielded results fully consistent with those obtained from EGCG solutions. Under HMT treatment conditions, cell lysates predominantly contained quinone metabolites (e.g., chrysin, m/z 255.2328, 255.2329), whereas MMT-treated conditions yielded predominantly enzyme metabolites (e.g., epicatechin, m/z 283.2643) (Figures S9 and S10, Supporting Information). These findings highlight the potential of EGCG-containing monotherapy for treating inflammation and cancer under MMT and HMT conditions, respectively.

The loading of EGCG and Fe_3O_4 in EGCG-Fe_3O_4 was confirmed by infrared spectroscopy and X-ray diffractometer (XRD) analysis (Figure S11, Supporting Information). Leveraging the inflammation-targeting property of M2-type macrophages, we opted to encapsulate EGCG-Fe_3O_4 NPs within MACs to further augment their curative effect (**Figure 2**A). After coating with high-purity MACs, a translucent membrane structure and variations in particle sizes and surface charges confirmed the successful acquisition of MAC@EGCG-Fe_3O_4 (Figure 2B,C; Figure S12, Supporting Information). The in vivo stability of NPs stands as a cornerstone in maximizing both drug bioavailability and biosafety. Apparently, MAC@EGCG-Fe_3O_4 demonstrated exceptional colloidal stability over a 5-day period at 37 °C in DMEM with fetal bovine serum, maintaining consistent hydrodynamic sizes, polydispersity indices (PDI), and zeta potentials throughout the observation window (Figure 2D,E).[34] As anticipated, Fe_3O_4 and EGCG-Fe_3O_4 suspensions revealed a durable and repeatable magnetothermal effect upon AMF irradiation (Figure 2F; Figures S13 and S14, Supporting Information). The release profiles of doxorubicin (DOX) from DOX-NPs and DOX-Fe_3O_4 NPs, in which DOX served as the model drug in place of EGCG, presented sustained drug release in response to pH, glutathione (GSH), hydrogen peroxide (H_2O_2), and AMF, demonstrating the responsive drug release properties of RSF-based NPs (Figure S15, Supporting Information).

Moreover, CLSM and flow cytometry (FCM) analyses demonstrated that coumarin 6 (Cou6)-labeled MAC@Fe_3O_4 nanoparticles (MAC@Cou6-Fe_3O_4) were rapidly internalized into RAW 264.7 macrophages and CT-26 cells, followed by efficient escape from their lysosomes, particularly with the aid of AMF irradiation (Figure 2G,H; Figures S16–S18, Supporting Information). Notably, the MAC coating significantly augmented the phagocytic uptake of MAC@Cou6-Fe_3O_4 by M1 macrophages, surpassing that observed in M2 macrophages. The colonic epithelial barrier is indispensable for separating the underlying mucosa from the hostile colon lumen and preventing unnecessary inflammatory responses by foreign substances.[35] Of note, MAC@EGCG-Fe_3O_4-mediated MMT achieved a substantial promotion of wound recovery (Figure 2I,J; Figure S19, Supporting Information). This treatment modality modulated inflammation-related proteins toward anti-inflammatory types.

Figure 1. Immunofluorescence analysis of clinical patient tissue samples and hematological data analysis. A) Schematic illustration of preparation and examination of the colon tissue samples from UC and CAC patients. This Figure was created with BioRender.com. Representative confocal images and their corresponding semi-quantitative MFIs of CD86 (M1-type macrophage marker) and CD206 (M2-type macrophage marker) in the colon tissues from B) UC patients and C) CAC patients. The cell nuclei were stained with DAPI. Scale bars: 100 µm. D)The dynamic light scattering (DLS) curve of EGCG-NPs showing hydrodynamic particle size distribution, polymer dispersity index (PDI), and zeta potential. E) Representative confocal images and their corresponding semi-quantitative MFIs of CD206 in the EGCG-NP-treated macrophages. The cell nuclei were stained with DAPI. Scale bar: 40 µm. F) Semi-quantitative MFIs of CD206 in macrophages receiving different treatments at 24, 48, and 72 h, respectively. G) Schematic illustration of the anti-inflammatory experimental design under different treatments. This Figure was created with BioRender.com. Concentrations of H) TNF-α and I) IL-10 in the supernatant of RAW 264.7 macrophages receiving different treatments for 24 h. J) The levels of hemoglobin (HGB), K) mean corpuscular volume (MCV), L) red cell distribution width (RDW), and M) ferritin in the serum of UC patients. Data are presented as means ± s.d. (healthy volunteers: 50 biologically independent samples; UC patients: 150 biologically independent samples). The levels of N) HGB, O) MCV, P) RDW, and Q) ferritin in the serum of CAC patients. Data are presented as means ± s.d. (healthy volunteers: 50 biologically independent samples; CAC patients: 51 biologically independent samples). One-way ANOVA with adjusted *p-value* in multiple comparison tests was used for statistical analysis.

© 2026 Wiley-VCH GmbH

15214095, 2026, 6, Downloaded from https://advanced.onlinelibrary.wiley.com/doi/10.1002/adma.202514413 by Universidade Do Minho, Wiley Online Library on [21/04/2026]. See the Terms and Conditions (https://onlinelibrary.wiley.com/terms-and-conditions) on Wiley Online Library for rules of use; OA articles are governed by the applicable Creative Commons License

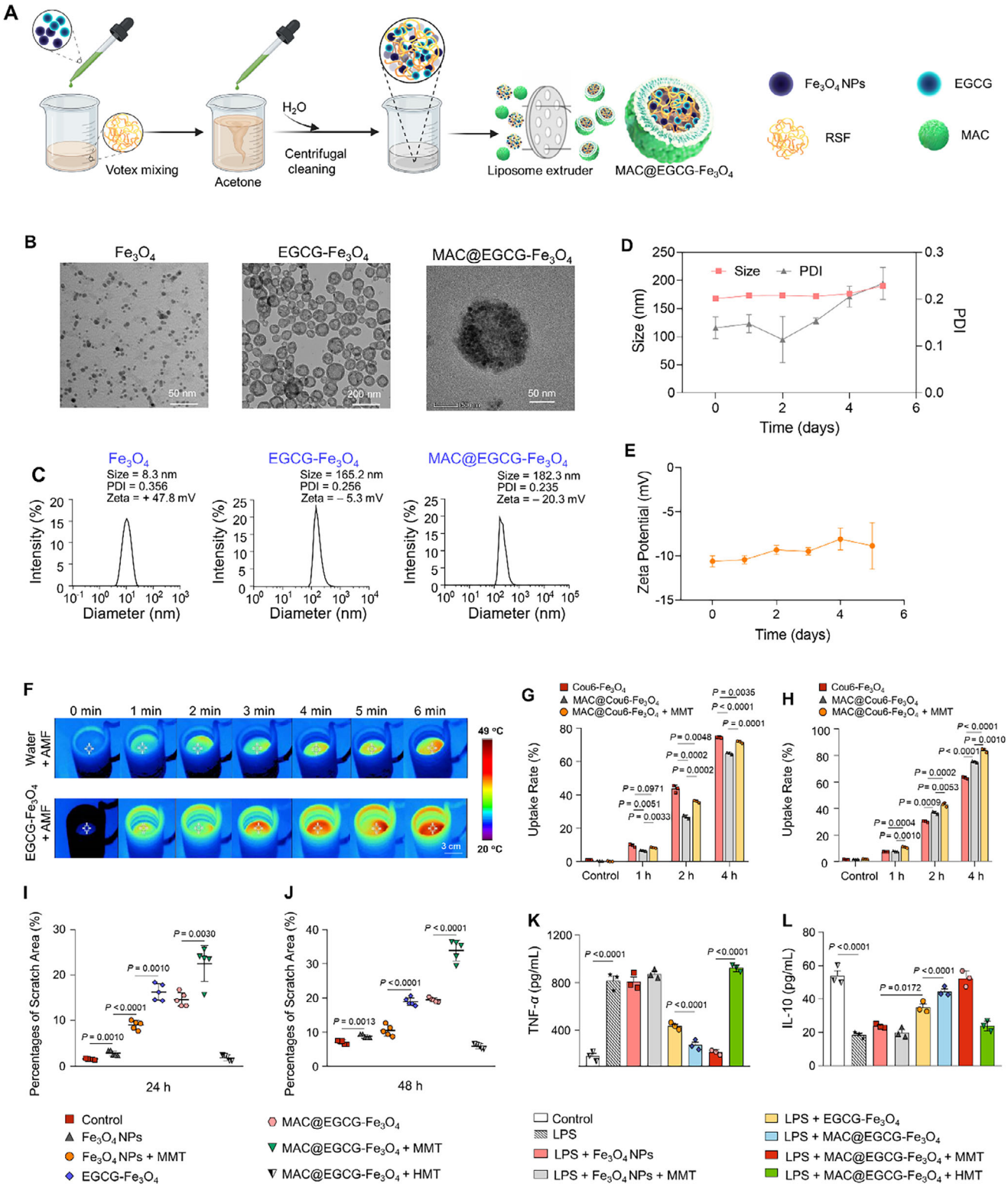


Figure 2. Design, preparation, and in vitro performance testing of MAC@EGCG-Fe_3O_4. A) Preparation diagram of MAC@EGCG-Fe_3O_4. EGCG: epigallocatechin gallate; RSF: regenerated silk fibroin; MAC: M2-type macrophage cell membrane. This Figure was created with BioRender.com. B) TEM images of Fe_3O_4, EGCG-Fe_3O_4, and MAC@EGCG- Fe_3O_4. Scale bars: 50/200 nm. C) The DLS curves of Fe_3O_4, EGCG- Fe_3O_4, and MAC@EGCG- Fe_3O_4 showing hydrodynamic particle size distribution, PDI, and zeta potential. Changes in D) size, PDI, and E) zeta potential of MAC@EGCG-Fe_3O_4 over 5 consecutive days in DMEM medium simulating in vivo conditions ($n = 3$ biologically independent samples). F) Thermal imaging images of water and EGCG-Fe_3O_4 treated with AMF for 6 min. Scale bar: 3 cm. Phagocytic efficiencies of Cou6-Fe_3O_4, MAC@Cou6-Fe_3O_4, and MAC@Cou6-Fe_3O_4 (+ MMT)

© 2026 Wiley-VCH GmbH

15214095, 2026, 6, Downloaded from https://advanced.onlinelibrary.wiley.com/doi/10.1002/adma.202514413 by Universidade Do Minho, Wiley Online Library on [21/04/2026]. See the Terms and Conditions (https://onlinelibrary.wiley.com/terms-and-conditions) on Wiley Online Library for rules of use; OA articles are governed by the applicable Creative Commons License

Instead, MAC@EGCG-Fe_3O_4 plus HMT stimulated the pro-inflammatory responses for CAC management (Figure 2K,L). The collective data suggests that MAC@EGCG-Fe_3O_4 holds great potential as a broad-spectrum therapeutic platform for UC and CAC by managing AMF durations.

2.3. AMF irradiation improves the accumulation of MAC@EGCG-Fe_3O_4 in colitis mucosa and colorectal tumor

Prior to studying the therapeutic effects of MAC@EGCG-Fe_3O_4 against colitis and its related colorectal cancer, we evaluated the optimal AMF duration. The whole-body infrared imaging revealed that only the mouse abdomen showed a temperature increase after receiving the treatment of MAC@EGCG-Fe_3O_4 plus AMF irradiation (Figure S20A,B, Supporting Information). Notably, hyperpyrexia induced by MAC@EGCG-Fe_3O_4 and AMF (4 min) caused apparent liver damage and inflammation, abnormal blood parameters (Figures S20C–I and S21, Supporting Information). Therefore, the MAC@EGCG-Fe_3O_4 plus MMT (AMF for 2 min) was selected for UC treatment, and MAC@EGCG-Fe_3O_4 plus HMT (AMF for 3 min) was considered more suitable for killing colorectal tumor cells.

Inspired by the inflamed tissue-targeting potential of M2-type macrophages, we investigated whether MAC@EGCG-Fe_3O_4 could selectively bind to the inflamed tissues. To track the distribution of MAC@EGCG-Fe_3O_4, we prepared NPs by loading with Cou6 or Cy7. As shown in **Figure 3**A,B, AMF significantly improved the locomotory capacity of MAC@Cou6-Fe_3O_4 and increased their infiltration depth in the artificial biological matrix, which would facilitate their deep penetration in the matrix of colitis mucosa and colorectal tumor tissues (Figure 3C,D). It was found that at the organ level, stronger fluorescent intensities were detected in the colons from UC and CAC mice receiving *ip* injection of MAC@Cy7-Fe_3O_4 compared with other groups (Figure 3E–H; Figure S20J–M, Supporting Information). Moreover, MAC@Cy7-Fe_3O_4, especially with AMF irradiation, effectively penetrated the deep colon tissues of UC and CAC mice (Figure 3I). Together, these data imply that AMF irradiation improves the accumulation of MAC@Cy7-Fe_3O_4 into the deep-seated colitis and colorectal tumor tissues after *ip* injection (Figure 3J).

2.4. MMT improves the therapeutic outcomes of MAC@EGCG-Fe_3O_4 against inflammation-associated colonic diseases

Subsequently, UC mice received *ip* injection of various NPs to screen for the best therapeutic strategy (**Figure 4**A). Administering MAC@EGCG-Fe_3O_4 plus MMT exerted alleviative interference on weight loss, colon shortening, and spleen index increase predominantly (Figure 4B,C; Figure S22A,B, Supporting Information). In contrast, other treatment modalities, including the clinically-used 5-ASA, exhibited diminished anticolitis outcomes. The endoscopic and histological analyses revealed noticeable ulcerative characteristics in the DSS control and all non-AMF groups. In contrast, the MAC@EGCG-Fe_3O_4 (+ MMT) group effectively mitigated colon ulcers (Figure 4D; Figure S22B, Supporting Information), which helped suppress the inflammatory reactions. This treatment not only decreased TNF-α levels and increased iron concentrations and IL-10 expressions but also reshaped macrophage polarization toward anti-inflammatory M2-phenotype in the inflamed colon (Figure 4D–I), which benefited the mitigation of inflammatory states and repair of the damaged colonic epithelial barrier. Precisely, the expression levels of 3 key tight junction-related proteins (MUC2, ZO-1, and Occludin) were significantly increased in the colitis tissues from the MAC@EGCG-Fe_3O_4 (+ MMT) group (Figure S22C–F, Supporting Information), confirming the restoration of intestinal barrier integrity. Beyond this, the in vivo biosafety of MAC@EGCG-Fe_3O_4 (+ MMT) treatment was guaranteed (Figures S23 and S24, Supporting Information).

The intestinal microbiota is closely associated with the development of gastrointestinal diseases.[36] To explore the potential of MAC@EGCG-Fe_3O_4 (+ MMT) in alleviating gut microbiota dysbiosis, we attempted to examine the temporal dynamics of the gut microbiome through 16S ribosomal RNA gene sequencing. Conspicuously, such treatment restored the DSS-induced decreased trend of microbial biodiversity and altered the bacterial composition of UC mice (Figure 4J; Figures S22G, and S25, Supporting Information). Unexpectedly, the overexpansion of harmful *Desulfovibrionaceae* (known for producing hydrothion that stimulates oxidative stress and destroys the intestinal mucosal barrier[37]) was terminated in the MAC@EGCG-Fe_3O_4 (+ MMT)-treated mice. On the contrary, the populations of beneficial *Enterorhabdus* and *Muribaculaceae*, known for their anti-inflammatory capacity to maintain intestinal homeostasis,[38,39] were increased (Figure 4K–M).

Alongside the gut microbiota's influence, the metabolites are intricately linked to UC progression.[40] Indeed, we discovered distinct metabolite compositions between the DSS control group and the MAC@EGCG-Fe_3O_4 (+ MMT) group, primarily enriched in choline metabolism, purine metabolism, and tryptophan metabolism (Figure S22H–J, Supporting Information). Several dysregulated metabolites were noticed in the volcano plot of these two groups, such as diacylglycerol (DAG), phosphoric acid (PA), cyclic adenosine monophosphate (cAMP), melatonin, and indole-3-ethanol (Figure S26, Supporting Information). Quantitatively, we uncovered that MAC@EGCG-Fe_3O_4 (+ MMT) treatment significantly increased the levels of DAG and PA in the choline metabolic pathway, which could inhibit macrophage polarization toward M1-phenotype by reducing iNOS expression and repairing the epithelial barrier by activating mTOR1 pathway.[41,42] Purine metabolism-involved cAMP, a secondary messenger that regulates the P38 pathway, was previously reported to promote the production of pro-inflammatory IL-6.[43,44]

by G) RAW 264.7 macrophages and H) CT-26 cells at the time points of 1, 2, and 4 h, respectively. Percentages of scratch areas of CT-26 cells receiving different treatments for I) 24 and J) 48 h, respectively. K) TNF-α and L) IL-10 concentrations in the supernatant of RAW 264.7 macrophages receiving different treatments for 24 h. Results of (I and J) (n = 5 biologically independent samples), and of (G, H, K, and L) (n = 3 biologically independent samples) are presented as means ± s.d. One-way ANOVA with adjusted *p-value* in multiple comparison tests was used for statistical analysis.

© 2026 Wiley-VCH GmbH

15214095, 2026, 6, Downloaded from https://advanced.onlinelibrary.wiley.com/doi/10.1002/adma.202514413 by Universidade Do Minho, Wiley Online Library on [21/04/2026]. See the Terms and Conditions (https://onlinelibrary.wiley.com/terms-and-conditions) on Wiley Online Library for rules of use; OA articles are governed by the applicable Creative Commons License

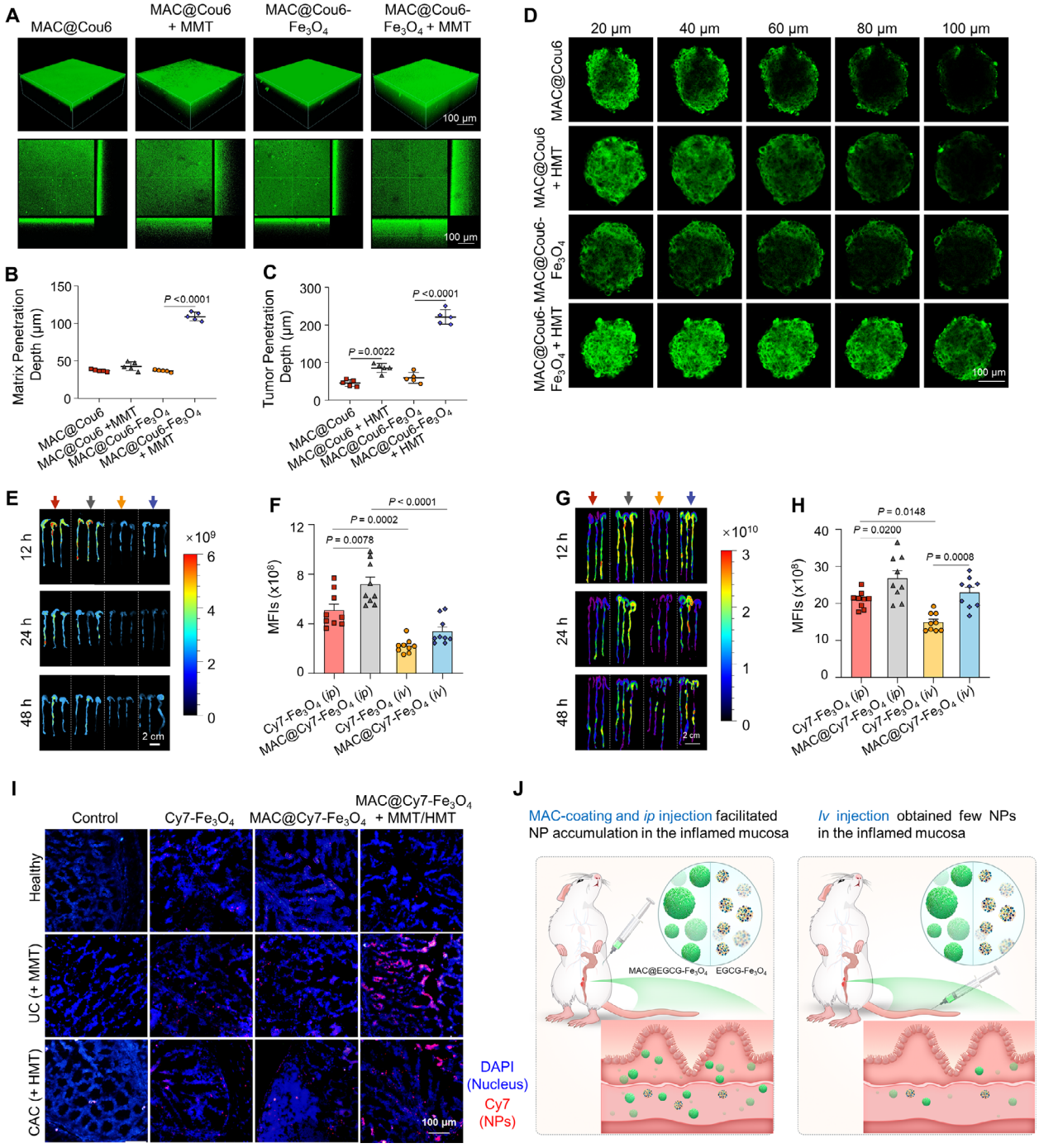
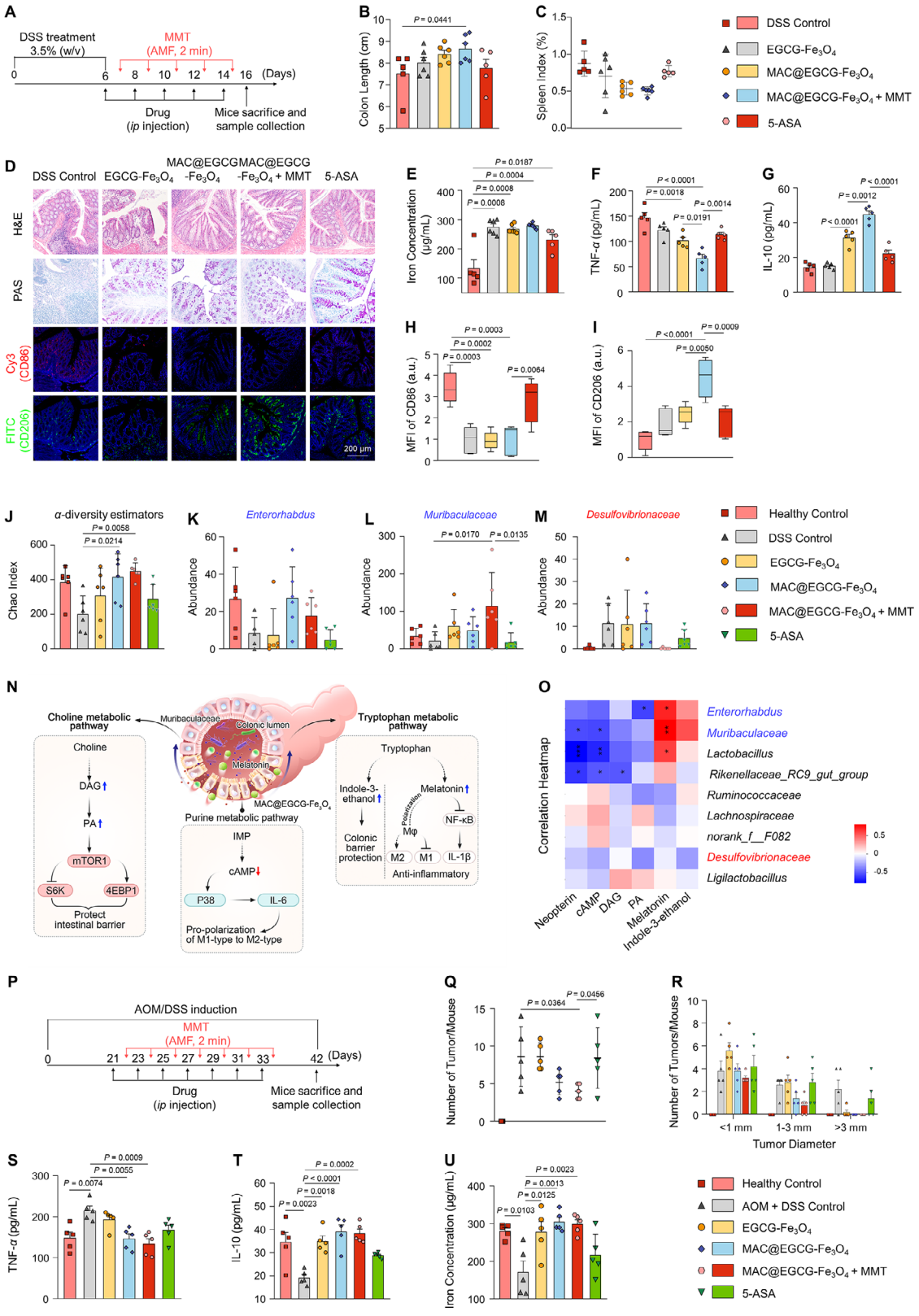


Figure 3. AMF increases the accumulation of MAC@Fe_3O_4 in the colitis mucosa and colorectal tumor tissues. A) Representative confocal images showing the penetration of MAC@Cou6-Fe_3O_4 (green) in the artificial matrix. Scale bars: 100 μm. B) The mean infiltration depth of MAC@Cou6 and MAC@Cou6-Fe_3O_4 with or without MMT irradiation in the artificial matrix. C) The penetration depth of MAC@Cou6 and MAC@Cou6-Fe_3O_4 with or without HMT irradiation into 3D CT-26 tumor spheroids, measured as the distance from the outer surface to the deepest point. D) Representative confocal images showing the distribution of MAC@Cou6 and MAC@Cou6-Fe_3O_4 (green) within 3D CT-26 tumor spheroids. Scale bar: 100 μm. E) Representative *ex vivo* fluorescence images of the colons from UC mice intravenously or intraperitoneally treated with Cy7-Fe_3O_4 and MAC@Cy7-Fe_3O_4 for 12, 24, and 48 h, respectively. Scale bar: 2 cm. F) Quantification of colon fluorescence intensities among different groups in UC mice. Three samples were collected at each time point (12, 24, and 48 h). G) Representative ex vivo fluorescence images of the colons from CAC mice collected at 12, 24, and 48 h postinjection of Cy7-Fe_3O_4 and MAC@Cy7-Fe_3O_4. Scale bar: 2 cm. H) Quantification of colon fluorescence intensities among different groups in CAC mice. Three samples were collected at each time point (12, 24, and 48 h). I) Representative confocal images showing the distribution of NPs in the colon tissues of UC/CAC mice following a 24-h *ip* injection of Cy7-Fe_3O_4 and MAC@Cy7-Fe_3O_4 with or without MMT/HMT irradiation. Scale bar: 100 μm. J) Schematic illustration showing the accumulation of Cy7-Fe_3O_4 and MAC@Cy7-Fe_3O_4 in the colon tissues following *ip*/*iv* injection. This Figure was created with BioRender.com. Results of (B and C) ($n = 5$ biologically independent samples), and of (F and H) ($n = 3$ biologically independent samples) are presented as means ± s.d. One-way ANOVA with adjusted *p-value* in multiple comparison tests was used for statistical analysis.

© 2026 Wiley-VCH GmbH

15214095, 2026, 6, Downloaded from https://advanced.onlinelibrary.wiley.com/doi/10.1002/adma.202514413 by Universidade Do Minho, Wiley Online Library on [21/04/2026]. See the Terms and Conditions (https://onlinelibrary.wiley.com/terms-and-conditions) on Wiley Online Library for rules of use; OA articles are governed by the applicable Creative Commons License



© 2026 Wiley-VCH GmbH

15214095, 2026, 6, Downloaded from https://advanced.onlinelibrary.wiley.com/doi/10.1002/adma.202514413 by Universidade Do Minho, Wiley Online Library on [21/04/2026]. See the Terms and Conditions (https://onlinelibrary.wiley.com/terms-and-conditions) on Wiley Online Library for rules of use; OA articles are governed by the applicable Creative Commons License

Its expression was significantly down-regulated by the treatment of MAC@EGCG-Fe_3O_4 (+ MMT), favoring inflammation remission. Tryptophan is an indispensable amino acid that can be metabolized into indole and melatonin.[45] A remarkable up-regulation existed in indole-3-ethanol, associated with intestinal barrier repair and intestinal function regulation, and melatonin, known for its anti-inflammatory effect by inhibiting the NF-κB pathway,[46–48] after *ip* injection of MAC@EGCG-Fe_3O_4 (+ MMT). Note that MAC@EGCG-Fe_3O_4 (+ MMT) treatment significantly suppressed neopterin abundance, a biomarker indicating macrophage-mediated immune activation, leading to alleviating intestinal inflammation (Figure 4N; Figure S22K–P and Table S1, Supporting Information).[49] These aberrantly expressed metabolites may be attributed to alterations in the abundance of *Muribaculaceae* and other bacteria (Figure 4O).[50]

Subsequently, we benchmarked the potential of MAC@EGCG-Fe_3O_4 plus MMT to retard the development of azoxymethane (AOM) and DSS-induced CAC (Figure 4P). Prominently, the treatment of MAC@EGCG-Fe_3O_4 (+ MMT) not only prevented tumor progression, with the fewest and most negligible tumor burdens, but also evaded the occurrence of DSS-induced inflammation and iron-deficiency, maintaining the expected levels of TNF-α, IL-10, and iron comparable to those in healthy mice (Figure 4Q–U).

2.5. HMT improves the therapeutic outcomes of MAC@EGCG-Fe_3O_4 ($\pm$ αPD-L1) against metastatic colorectal tumors and their recurrence

Due to the favorable in vitro antitumor effect of MAC@EGCG-Fe_3O_4 (+ HMT), we further assessed its anticolorectal tumor efficacy in the presence or absence of αPD-L1 (**Figure 5A**). Alongside being nontoxic (Figure S27, Supporting Information), two HMT-involved groups owned a remarkable tumor regression (Figure 5B–D,G; Figure S28A–D, Supporting Information). The combination of MAC@EGCG-Fe_3O_4 (+ HMT) and αPD-L1 increased the levels of pro-inflammatory TNF-α and IFN-γ, benefitting the activation, mobilization, and expansion of immune cells (Figure 5E,F). To validate its significance in activating antitumor immunity, we measured the subpopulations of typical immune cells, including macrophages, cytotoxic T lymphocytes (e.g., $CD4^+$ and $CD8^+$ T cells), as well as mature DCs (mDCs, $CD80^+CD86^+$). The treatment of MAC@EGCG-Fe_3O_4 (+ HMT + αPD-L1) reprogrammed macrophages to a healthy state and increased the levels of proliferative CD8+ T cells and thymus-resident mDCs, effectively enhancing immune-supportive components without causing systemic adverse effect (Figure 5H–J; Figures S28A,E,F and S29–S31, Supporting Information).

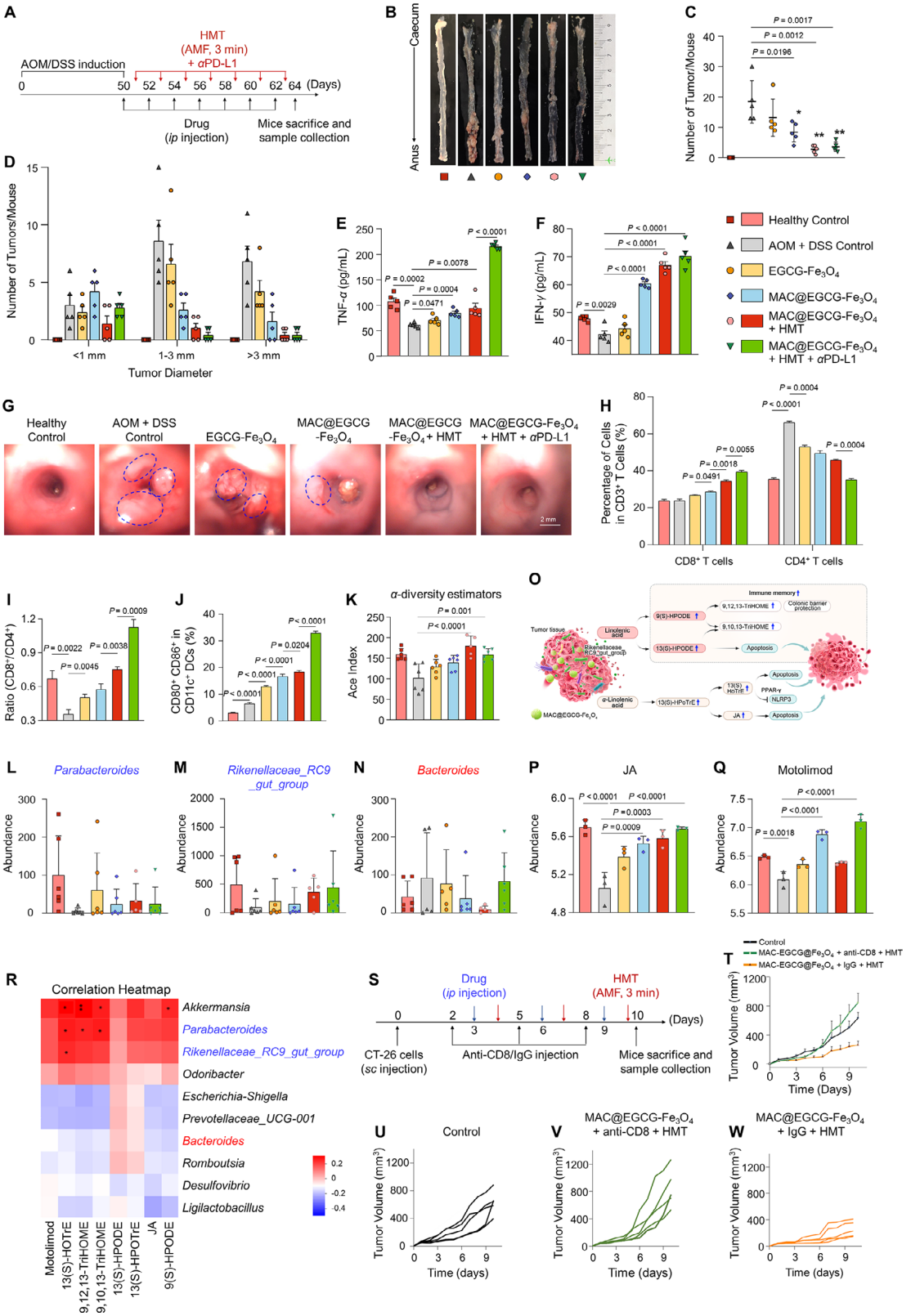
Significantly, two HMT-involved groups also corrected the imbalanced intestinal microbe compositions (Figure 5K; Figures S28G and S32, Supporting Information). In particular, MAC@EGCG-Fe_3O_4 (+ HMT + αPD-L1) treatment increased the abundance of beneficial *Parabacteroides* and *Rikenellaceae_RC9_gut_group*, while reducing the proportion of detrimental *Bacteroides*, which helped inhibit the growth of colorectal tumors (Figure 5L–N). Benefited by gut microbiome modulation, the fecal metabolites exhibited noticeable discrepancies between the AOM + DSS control group and the MAC@EGCG-Fe_3O_4 (+ HMT + αPD-L1) group, mainly related to α-linolenic acid metabolism and linoleic acid metabolism (Figure S28H-J, Supporting Information). The activation of linoleic acid metabolism directly caused tumor cell apoptosis and indirectly eliminated tumor cells by activating immune memory.[51,52] After treatment with MAC@EGCG-Fe_3O_4 (+ HMT + αPD-L1), there was a significant upregulation of its representative metabolites, particularly 13(S)-HPODE (Figure 5O). Moreover, this treatment also increased the abundance of metabolites related to α-linolenic acid metabolism, such as 13(S)-HPoTrE and jasmonic acid (JA), which could act as inducers for tumor cell apoptosis.[53–55] In this group, we noticed an additional up-regulated metabolite called motolimod, which functioned as a TLR8 agonist to enhance anti-tumor immunity by promoting the activity of T cells and natural killer cells.[56] These beneficial metabolites significantly correlate with certain bacteria, especially *Parabacteroides* and *Rikenellaceae_RC9_gut_group* (Figure 5P–R; Figures S28K-P and S33, and Table S2, Supporting Information).

To certify the importance of antitumor CD8+ T cells in MAC@EGCG-Fe_3O_4 (+ HMT + αPD-L1)-mediated tumor attenuation, anti-CD8 antibodies were injected intraperitoneally to exhaust CD8+ T cells in subcutaneous CT-26 tumor-bearing mice (Figure 5S; Figure S34, Supporting Information). After depleting CD8+ T cells, the inhibitory effect of MAC@EGCG-Fe_3O_4 (+ HMT + αPD-L1) on tumor growth was significantly weakened than the IgG-involved group (Figure 5T–W), suggesting that this therapeutic modality could activate innate and adaptive immunity and inhibit tumor growth. The activation of the adaptive immune responses by MAC@EGCG-Fe_3O_4

Figure 4. In vivo therapeutic effect of MAC@EGCG-Fe_3O_4 plus MMT (AMF, 2 min) against UC and CAC. A) Experimental design of the UC mouse model for in vivo investigation. B) Colon lengths and C) spleen indices of UC mice after different treatments. D) Representative H&E, PAS, and fluorescence staining images of the colon tissues from different groups. The cell nuclei were stained with DAPI. Scale bar: 200 μm. E) Concentrations of iron ions in the serum from UC mice after different treatments. F) TNF-α and G) IL-10 concentrations in the serum of UC mice after different treatments. Semi-quantitative MFIs of H) CD86-positive and I) CD206-positive areas in the colon tissues from UC mice after different treatments. J) Chao indices on the OTU level of microbiota from different groups. Relative abundances of K) *Enterorhabdus*, L) *Muribaculaceae*, and M) *Desulfovibrionaceae* from different groups. N) Schematic illustration showing the impacts of choline metabolism, purine metabolism, and tryptophan metabolism pathways on UC and the underlying therapeutic molecular mechanism of MAC@EGCG-Fe_3O_4 (+ MMT). This Figure was created with BioRender.com. O) Spearman correlations between intestinal microbiota and metabolites in the MAC@EGCG-Fe_3O_4 (+ MMT) group versus the DSS control group. The label in red indicates a positive correlation, while the label in blue indicates a negative correlation. The color intensities are proportional to Spearman correlation strengths ($^*p < 0.05$, $^{**}p < 0.01$, and $^{***}p < 0.001$). P) Experimental design of the CAC mouse model for in vivo investigation. Q) Orthotopic tumor numbers and R) tumor size distribution of different groups at the end of investigations. Concentrations of S) TNF-α, T) IL-10, and U) iron ions in the serum from different groups. Results of (B, C, E and K–M) (n = 5-6 biologically independent samples), (J) (n = 6 biologically independent samples) and of (F to I and Q to U) (n = 5 biologically independent samples) are presented as means ± s.d. One-way ANOVA with adjusted *p-value* in multiple comparison tests was used for statistical analysis.

© 2026 Wiley-VCH GmbH

15214095, 2026, 6, Downloaded from https://advanced.onlinelibrary.wiley.com/doi/10.1002/adma.202514413 by Universidade Do Minho, Wiley Online Library on [21/04/2026]. See the Terms and Conditions (https://onlinelibrary.wiley.com/terms-and-conditions) on Wiley Online Library for rules of use; OA articles are governed by the applicable Creative Commons License



© 2026 Wiley-VCH GmbH

15214095, 2026, 6, Downloaded from https://advanced.onlinelibrary.wiley.com/doi/10.1002/adma.202514413 by Universidade Do Minho, Wiley Online Library on [21/04/2026]. See the Terms and Conditions (https://onlinelibrary.wiley.com/terms-and-conditions) on Wiley Online Library for rules of use; OA articles are governed by the applicable Creative Commons License

(+ HMT + αPD-L1) further prompted us to investigate its potential for immune memory. After anti-tumor treatment, the immunized orthotopic CAC mice received subcutaneous CT-26 tumor rechallenge on day 71 (**Figure 6A**). Apart from effectively suppressing orthotopic colorectal tumor growth and reprogramming macrophage polarization (Figure 6B–D; Figure S35, Supporting Information), MAC@EGCG-Fe_3O_4 (+ HMT + αPD-L1) immunization completely prevented colorectal tumor attacks (Figure 6E–K). Meanwhile, this treatment modality also elevated the iron and TNF-α levels in the serum to the highest values (Figure 6L,M). More importantly, we observed significant increases in the proportion of central memory T cells ($CD44^{high}$ $CD62L^+$) within both $CD4^+$ and $CD8^+$ T cell subsets in splenocytes from the MAC@EGCG-Fe_3O_4 (+ HMT + αPD-L1)-treated mice, indicating that this treatment could activate a strong systemic anti-tumor immune response against tumor metastasis and recurrence (Figure 6N–U; Figure S36, Supporting Information). Collectively, the above findings demonstrate that the treatment of MAC@EGCG-Fe_3O_4 (+ HMT + αPD-L1) can effectively elicit innate/adaptive immunity and immune memory, which is crucial for inhibiting colorectal tumor growth and achieving long-term prevention of tumor recurrence.

3. Discussion

UC is a chronic inflammatory disorder of the gastrointestinal tract with a potential risk for developing CAC.[3] To address the symptoms of colitis and its associated colorectal cancer, we rationally designed a dual-role nanomedicine—MAC@EGCG-Fe_3O_4—coated with M2 macrophage membranes based on the inflammation-homing capability of M2-type macrophages and the therapeutic potential of magnetothermia in the treatment of inflammatory diseases and cancers. It has been noted that when combined with MMT, MAC@EGCG-Fe_3O_4 notably ameliorated UC symptoms by repolarizing macrophages, reducing intestinal inflammation, scavenging ROS/RNS, supplementing iron, and restoring both intestinal barrier function and microbiota composition. It also induced a notable metabolic reprogramming, recognized as a crucial mechanism for intricately modulating the activation, differentiation, and functionality of immune cells. By influencing the choline, purine, and tryptophan metabolism pathways, several representative metabolites (e.g., DAG, PA, cAMP, melatonin, and indole-3-ethanol) were altered following the treatment of MAC@EGCG-Fe_3O_4 (+ MMT), benefiting colonic epithelial barrier restoration and macrophage repolarization. In addition to treating UC, MAC@EGCG-Fe_3O_4 elicited pro-inflammatory responses for CAC therapy when combined with AMF-induced hyperpyrexia (HMT). In vivo study of MAC@EGCG-Fe_3O_4 combined with HMT and αPD-L1 demonstrated remarkable tumor regression and prevention by ablating tumors, activating long-term immune memory, and rectifying microbial metabolites (e.g., 13(S)-HPODE).

Although previous studies have made significant progress in treating UC and CAC by modulating the inflammatory microenvironment and scavenging ROS,[57–59] our work pioneers a pathology-driven therapeutic paradigm that transcends conventional material-or physicochemical property-dependent designs. Specifically, we exploit macrophage chemotaxis, naturally guided by pathological cues within inflamed tissues, to achieve precise site-specific delivery. Furthermore, recognizing the prevalent iron deficiency in UC and CAC patients, we strategically incorporate Fe_3O_4 not only as an iron source but also as a magnetothermal transducer capable of mediating localized thermal therapy under external AMF stimulation. Crucially, the integration of EGCG introduces a thermoresponsive redox switch, enabling dynamic, on-demand regulation between ROS scavenging and controlled generation—its activity finely tuned by temperature. In contrast to traditional approaches, our dual-regulated platform provides unique spatiotemporal precision and flexibility, thereby establishing a conceptually innovative blueprint for next-generation treatment of UC and CAC. Overall, the MAC@EGCG-Fe_3O_4 is a broad-spectrum treatment platform for targeted treatment of both UC and CAC by precisely manipulating the AMF duration, opening up a new avenue for treating inflammation and related diseases.

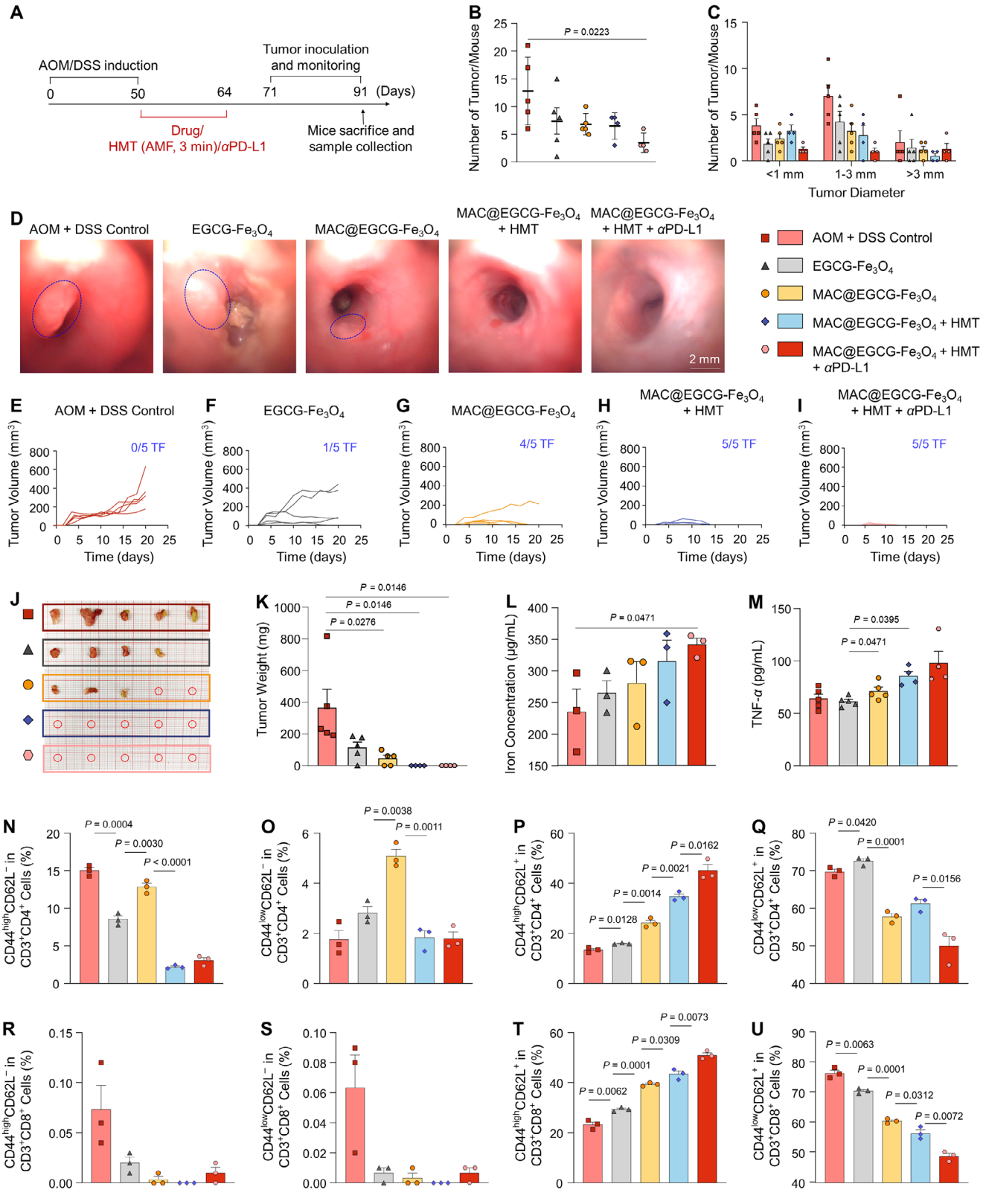
4. Experimental Section

Macrophage Profiles of the Colon Tissues from Patients with UC and CAC: Human colon tissue sections were obtained from patients with UC or CAC in the First Affiliated Hospital of Nanchang University (Nanchang, China) following ethical guidelines and approved by the Institutional Review Board under the approval number of (2023) CDYFYYLK (02-029). The sections (n = 40 samples) consisted of 8 subgroups (n = 5 per group): healthy, UC (varying degrees), and CAC (various stages). The sections were stained with fluorescently labeled anti-human CD206 and CD86 antibodies to assess the distribution of macrophages, and the images were

Figure 5. In vivo therapeutic outcomes of MAC@EGCG-Fe_3O_4 plus HMT (AMF, 3 min) and αPD-L1 against orthotopic CAC. A) Experimental design of establishing a CAC mouse model and the treatment processes. B) Ex vivo colon images of CAC mice from different groups. C) Orthotopic tumor numbers and D) tumor size distributions of different groups at the end of the investigations. E) TNF-α and F) IFN-γ concentrations in the serum from different groups. G) Endoscopic images of mice in different groups on day 64. Scale bar: 2 mm. H) Percentages of $CD3^+$ $CD8^+$ T cells and $CD3^+$ $CD4^+$ T cells in the spleens from different groups. I) Ratios of $CD8^+/CD4^+$ T cells in the spleens from different groups. J) Percentages of $CD80^+$ $CD86^+$ cells in $CD11c^+$ DCs in the thymuses from different groups. K) Ace indices on OTU level of microbiota from different groups. Relative abundances of L) *Parabacteroides*, M) *Rikenellaceae_RC9_gut_group*, and N) *Bacteroides* from different groups. O) Schematic illustration showing the impacts of linoleic acid metabolism and α-linolenic acid pathways on the development of CAC and the underlying therapeutic molecular mechanism of MAC@EGCG-Fe_3O_4 (+ HMT + αPD-L1). This Figure was created with BioRender.com. Relative abundances of P) JA and Q) motolimod from different groups. R) Spearman correlations between intestinal microbiota and metabolites in the MAC@EGCG-Fe_3O_4 (+ HMT + αPD-L1) group versus the DSS control group. The label in red indicates a positive correlation, while the label in blue indicates a negative correlation. The color intensities are proportional to the Spearman correlation strengths ($^*p < 0.05$, $^{**}p < 0.01$, and $^{***}p < 0.001$). S) Experimental design of anti-tumor assessment in the CT-26-bearing mice after CD8+ T cell depletion. T) Tumor growth profiles of different groups. Individual tumor growth profiles of CT-26 tumors from mice treated with U) PBS, V) MAC@EGCG-Fe_3O_4 (+ anti-CD8 + HMT), and W) MAC@EGCG-Fe_3O_4 (+ IgG + HMT). Results of (C to F and U to W) (n = 5 biologically independent samples), (K–N) (n = 5-6 biologically independent samples) and (H to J and P, Q) (n = 3 biologically independent samples) are presented as means ± s.d. One-way ANOVA with adjusted *p-value* in multiple comparison tests was used for statistical analysis.

© 2026 Wiley-VCH GmbH

15214095, 2026, 6, Downloaded from https://advanced.onlinelibrary.wiley.com/doi/10.1002/adma.202514413 by Universidade Do Minho, Wiley Online Library on [21/04/2026]. See the Terms and Conditions (https://onlinelibrary.wiley.com/terms-and-conditions) on Wiley Online Library for rules of use; OA articles are governed by the applicable Creative Commons License



© 2026 Wiley-VCH GmbH

15214095, 2026, 6, Downloaded from https://advanced.onlinelibrary.wiley.com/doi/10.1002/adma.202514413 by Universidade Do Minho, Wiley Online Library on [21/04/2026]. See the Terms and Conditions (https://onlinelibrary.wiley.com/terms-and-conditions) on Wiley Online Library for rules of use; OA articles are governed by the applicable Creative Commons License

acquired using a confocal laser scanning microscope (CLSM, FV3000, Olympus Corporation, Japan).

Blood Indices of Human Patients: The human blood index data were collected from the Sixth Affiliated Hospital of Sun Yat-sen University in Guangdong Province, China (Ethical approval number: E2024064), the Second Affiliated Hospital of Army Military Medical University in Chongqing Province, China (Ethical approval number: 2024-clinical research 304), and the Second Affiliated Hospital of Chongqing Medical University in Chongqing Province, China (Ethical approval number: science [2024] 307). The data comprised 251 samples divided into eight subgroups, encompassing individuals with normal health, varying degrees of UC, and different stages of CAC.

Fabrication of EGCG-NPs and EGCG-Fe_3O_4-NPs: The EGCG-NPs were prepared as previously reported.[60] Briefly, a mixed solution containing EGCG (10 mg), RSF (150 mg), and deionized water (10 mL) was prepared. Subsequently, the mixed solution was added dropwise into acetone under gentle stirring to form emulsions. After vortexing for 30 seconds and homogenizing with an ultrasound probe for 1 min, the emulsions were stirred in a well-ventilated facility for 2 h. The final product (EGCG-NPs) was centrifuged (13 000 *g*, 18 min) and washed 3 times with water.

The synthesis of EGCG-Fe_3O_4-NPs was conducted following the procedure mentioned above. Likewise, EGCG (10 mg) and Fe_3O_4 NPs (20 mg) were fully suspended in RSF solution (1.5%, w/v; 10 mL). After being added to acetone to form emulsions, the organic solvent was evaporated in a well-ventilated facility. The final EGCG-Fe_3O_4-NPs were gathered by centrifugation (13 000 *g*, 18 min) after washing with water 3 times.

Synthesis of MAC@EGCG-Fe_3O_4: Initially, the M2 phenotype MAC was extracted from well-grown M2-phenotype RAW 264.7 macrophages induced by recombinant murine IL-4 (Beyotime, Shanghai, China), as follows: The M2-phenotype RAW 264.7 macrophages were harvested, centrifuged (700 *g*, 7 min), and resuspended in a buffer (pH 7.0) composed of Tris-HCl (30 mM), sucrose (76 mM), D-mannitol (225 mM), and 1× proteinase phosphatase inhibitor. After homogenization for 6 min, cells were centrifuged (10 000 *g*, 25 min) at 4 °C to collect the supernatant containing cell membranes, which was centrifuged at 150 000 *g* for 35 min to obtain the precipitated MAC. The precipitate was resuspended in enzyme-free water containing EDTA (0.2 mM), and the membrane proteins were quantified using the BCA kit. The collected MAC and unpurified cell homogenates were subjected to sonication and stained with DAPI for a membrane purity assay using CLSM observation (FV3000, Olympus Corporation, Japan).

MAC@EGCG-Fe_3O_4 NPs were synthesized via membrane extrusion. The EGCG-Fe_3O_4-NPs (10 mg) were added to the MAC suspension (1 mg membrane protein) and extruded through 400 and 200 nm polycarbonate membrane filters to form MAC@EGCG-Fe_3O_4 NPs. The iron content in MAC@EGCG-Fe_3O_4 NPs was determined by completely dissolving NPs (10 mg) in aqua regia (1 mL) for 24 h, followed by detection using an inductively coupled plasma emission spectrometer (NexION 1000G, PerkinElmer, USA) after a 1000-fold dilution.

Therapeutic Outcomes of MAC@EGCG-Fe_3O_4 Plus Mild AMF Against DSS-Induced UC: BALB/c mice (female, 6-8 weeks old) were obtained from Chongqing Ensville Biotechnology Co., Ltd. (Chongqing, China). The DSS-induced UC mice were randomly divided into five groups, namely the DSS control group, the EGCG-Fe_3O_4 group, the MAC@EGCG-Fe_3O_4 group, the MAC@EGCG-Fe_3O_4 (+ AMF) group, and the 5-ASA group. The mice were intraperitoneally injected with various formulas (EGCG: 5 mg per kg) or orally administered with 5-ASA (30 mg per kg) every two days. At 24 h postadministration, the AMF-involved group was exposed to AMF (5 kW) for 2 min. The body weights of mice were monitored throughout the entire treatment. On day 15, the mouse colons were examined via endoscopy (Chemidoc Touch, Bio-Rad, USA). On day 16, mice were sacrificed, and their blood was collected to measure cytokine expression levels (TNF-α, IL-6, and IL-10) in the serum. The colon tissues and five principal organs were harvested; the colon lengths and organ indices were measured; and histological H&E staining was performed. Colonic MPO activities were measured using the corresponding kit.

Mucus in the colon tissue was stained with PAS and quantified using Image-Pro Plus software. Tissues were subjected to immunofluorescence staining using specific antibodies, such as CD206, CD86, MUC2, Occludin, and ZO-1 for CLSM observation (FV3000, Olympus Corporation, Japan) to investigate the macrophage polarization and epithelial barrier repair in the colon tissues. The fecal samples were collected and sent to Majorbio Bio-Pharm Technology (Shanghai, China) for microbiome and metabolome analysis.

Therapeutic Outcomes of MAC@EGCG-Fe_3O_4 Plus Hyperpyrexia AMF and αPD-L1 Against Orthotopic CAC: BALB/c mice (female, 6–8 weeks old) were obtained from Chongqing Ensville Biotechnology Co., Ltd. (Chongqing, China). The CAC mice were randomly divided into five groups, namely the AOM-DSS control group, the EGCG-Fe_3O_4 group, the MAC@EGCG-Fe_3O_4 group, the MAC@EGCG-Fe_3O_4 (+ AMF) group, the MAC@EGCG-Fe_3O_4 (+ AMF + αPD-L1) group, and intraperitoneally received NPs (EGCG: 5.0 mg kg^{-1}) every 2 days. After 24 h of NP injection, mice were subjected to AMF irradiation (5 kW, 3 min) and intravenously administered with αPD-L1 solution (2.5 mg kg^{-1}). Healthy mice served as the control. At regular intervals, mouse body weights were recorded. The mouse colons were examined by an endoscope (H3, YUYAN instruments, China) prior to the end of the experiments. After that, the mice were euthanized, and their principal organs were collected for histological examination and immune analysis. The collected blood samples were utilized to determine TNF-α and IFN-γ serum levels. The mature DCs were quantified by performing FCM (CYTOFLEX, Beckman Coulter, USA) analysis on the cells extracted from the thymuses, which were co-stained with anti-mouse CD11c-FITC, anti-mouse CD80-APC/Fire 750, and anti-mouse CD86-PE antibodies. To quantify the T cell phenotypes and memory T cell phenotypes, cells extracted from the spleens were stained with anti-CD3-FITC, anti-CD4-PE, anti-CD4-PERCP, anti-CD8α-PERCP-Cy5.5, anti-CD44-APC, and anti-CD62L-PE antibodies for FCM analysis.

Therapeutic Outcomes of MAC@EGCG-Fe_3O_4 Plus Hyperpyrexia AMF and αPD-L1 Against Orthotopic CAC and Distant Colorectal Tumors: BALB/c mice (female, 6–8 weeks old) were obtained from Chongqing Ensville Biotechnology Co., Ltd. (Chongqing, China). CAC mice received the treatment of EGCG-Fe_3O_4, MAC@EGCG-Fe_3O_4, MAC@EGCG-Fe_3O_4 (+ AMF), and MAC@EGCG-Fe_3O_4 (+ AMF + αPD-L1), and CT-26 cells were subcutaneously injected into the right flank of each mouse on day 71. Body weights and subcutaneous tumor volumes were recorded every day. The mouse colons were examined by an endoscope (H3, YUYAN instruments, China) before the end of the experiments. On day 91, the mice were euthanized, and their blood and primary tissues were collected for histological examination, immunofluorescence staining, and immune analysis, including TNF-α detection, as well as quantification of T cell phenotypes and memory T cell phenotypes.

Figure 6. Tumor rechallenge of CAC mice treated with MAC@EGCG-Fe_3O_4 plus HMT and αPD-L1. A) Experimental design of orthotopic and distant colorectal tumor models and the treatment processes. B) Orthotopic tumor numbers and C) tumor size distributions of different groups at the end of the investigations. D) Endoscopic images of mice in different groups on day 91. Scale bar: 2 mm. Individual subcutaneous tumor growth profiles of mice receiving the treatment of E) PBS, F) EGCG-Fe_3O_4, G) MAC@EGCG-Fe_3O_4, H) MAC@EGCG-Fe_3O_4 (+ HMT), and I) MAC@EGCG-Fe_3O_4 (+ HMT + αPD-L1). TF: tumor-free. J) Representative subcutaneous tumor images and K) tumor weights of different groups. L) Concentrations of iron ions in the serum from different groups. M) Concentrations of TNF-α in the serum from different groups. Statistical data on the percentages of N) $CD44^{high}$ $CD62L^{-}$, O) $CD44^{low}$ $CD62L^{-}$, P) $CD44^{high}$ $CD62L^{+}$, and Q)$CD44^{low}$ $CD62L^{+}$ in $CD3^{+}$ $CD4^{+}$ T cells from the spleens of different groups. Statistical data on the percentages of R) $CD44^{high}$ $CD62L^{-}$, S) $CD44^{low}$ $CD62L^{-}$, T) $CD44^{high}$ $CD62L^{+}$, and U) $CD44^{low}$ $CD62L^{+}$ in $CD3^{+}$ $CD8^{+}$ T cells from the spleens of different groups. Results of (B, C, J, K and M) (n = 4-5 biologically independent samples), (L–U) (n = 3 biologically independent samples) and (E to I) (n = 5 biologically independent samples) are presented as means ± s.d. One-way ANOVA with adjusted *p-value* in multiple comparison tests was used for statistical analysis.

© 2026 Wiley-VCH GmbH

15214095, 2026, 6, Downloaded from https://advanced.onlinelibrary.wiley.com/doi/10.1002/adma.202514413 by Universidade Do Minho, Wiley Online Library on [21/04/2026]. See the Terms and Conditions (https://onlinelibrary.wiley.com/terms-and-conditions) on Wiley Online Library for rules of use; OA articles are governed by the applicable Creative Commons License

Statistical Analysis: All data were analyzed using GraphPad Prism (version 9.0, GraphPad Software, San Diego, CA, USA) unless otherwise specified. Data pre-processing involves normalization, where applicable, and assessment of outliers. Data are presented as mean ± standard error of the mean (s.d.), unless otherwise indicated. Experiments were conducted with a minimum of three independent biological replicates, and each assay was performed in technical duplicate or triplicate to ensure reliability and reproducibility. For comparisons involving more than two groups, one-way analysis of variance (ANOVA) was conducted, followed by Tukey's post hoc test to determine statistical significance. All *p*-values reported in figure legends correspond to a significance level of $\alpha = 0.05$. Flow cytometry data were analyzed using FlowJo (version 10, BD Biosciences, Franklin Lakes, NJ, USA), and colocalization coefficients were quantified using ImageJ (version 1.54f, NIH, Bethesda, MD, USA) with the Coloc2 plugin. Data are presented using bar plots with individual data points, box-and-whisker plots, or fluorescence quantification graphs, as appropriate. All figures include annotations specifying the statistical test used, the sample size (n), the type of comparisons performed, and *p* values to ensure transparency, reproducibility, and compliance with statistical reporting standards.

Supporting Information

Supporting Information is available from the Wiley Online Library or from the author.

Acknowledgements

This study was supported by the National Natural Science Foundation of China (82472132 and 32401170), Chongqing Natural Science Foundation (CSTB2023NSCQ-MSX0422), the Chongqing Municipal Financial Fund Project (24506C), the Distinguished Young Scholars of Chongqing (2022NSCQ-JQX5279), the Science and Technology Research Program of Chongqing Municipal Education Commission (KJQN202300223), and Sichuan Science and Technology Program (2024YFFK0345).

Conflict of Interest

The authors declare no conflict of interest.

Author Contributions

S.L. and B.L. contributed equally to this work. X.S., G.N., and B.X. designed and supervised the project. S.L., B.L., Q.Y., M.Z., H.X., B.L., and X.Y. performed experiments and analyzed data. P.L., J.Z., L.L., Z.Z., and X.P. collected human patient data. M.S., R.L.R., and S.C.K. provided advice and revised the manuscript. X.S., G.N., and B.X. directed the studies and wrote the manuscript with S.L. and B.L. All authors approved the final version of the manuscript.

Data Availability Statement

The data that support the findings of this study are available in the supplementary material of this article.

Keywords

alternating magnetic field therapy, colitis-associated colorectal cancer, macrophage membrane coating, nanomedicine, ulcerative colitis

Received: July 26, 2025
Revised: September 27, 2025
Published online: November 11, 2025

[1] M. F. Neurath, *Nat. Rev. Immunol.* **2024**, *24*, 559.
[2] M. Wang, R. Cha, W. Hao, X. Jiang, *ACS Nano* **2023**, *17*, 18965.
[3] W. H. Yang, D. M. Heithoff, P. V. Aziz, M. Sperandio, V. Nizet, M. J. Mahan, J. D. Marth, *Science* **2017**, *358*, aao5610.
[4] P. Guo, W. Wang, Q. Xiang, C. Pan, Y. Qiu, T. Li, D. Wang, J. Ouyang, R. Jia, M. Shi, Y. Wang, J. Li, J. Zou, Y. Zhong, J. Zhao, D. Zheng, Y. Cui, G. Ma, W. Wei, *Cell Host Microbe* **2024**, *32*, 1502.
[5] N. Nakamoto, N. Sasaki, R. Aoki, K. Miyamoto, W. Suda, T. Teratani, T. Suzuki, Y. Koda, P.-S. Chu, N. Taniki, A. Yamaguchi, M. Kanamori, N. Kamada, M. Hattori, H. Ashida, M. Sakamoto, K. Atarashi, S. Narushima, A. Yoshimura, K. Honda, T. Sato, T. Kanai, *Nat. Microbiol.* **2019**, *4*, 492.
[6] A. E. Jacobson-Kelly, J. R. Stanek, J. M. Powers, S. H. O'Brien, *Blood* **2018**, *132*, 3507.
[7] Y. Chen, J. Liang, S. Chen, N. Lin, S. Xu, J. Miao, J. Zhang, C. Chen, X. Yuan, Z. Xie, E. Zhu, M. Cai, X. Wei, S. Hou, H. Tang, *Mol. Cancer* **2024**, *23*, 196.
[8] N. Kakiuchi, K. Yoshida, M. Uchino, T. Kihara, K. Akaki, Y. Inoue, K. Kawada, S. Nagayama, A. Yokoyama, S. Yamamoto, M. Matsuura, T. Horimatsu, T. Hirano, N. Goto, Y. Takeuchi, Y. Ochi, Y. Shiozawa, Y. Kogure, Y. Watatani, Y. Fujii, S. K. Kim, A. Kon, K. Kataoka, T. Yoshizato, M. M. Nakagawa, A. Yoda, Y. Nanya, H. Makishima, Y. Shiraishi, K. Chiba, et al., *Nature* **2020**, *577*, 260.
[9] J. Kim, G. Ryu, J. Seo, M. Go, G. Kim, S. Yi, S. Kim, H. Lee, J. Y. Lee, H. S. Kim, M. Park, D. H. Shin, H. Shim, W. Kim, S. Y. Lee, *Nat. Commun.* **2024**, *15*, 1024.
[10] T. Meng, J. Zheng, M. Chen, Y. Zhao, H. Sudarjat, M. R. Aji Alex, V. Kulkarni, Y. Oh, S. Xia, Z. Ding, H. Han, N. Anders, M. A. Rudek, W. Chow, W. Stark, L. M. Ensign, J. Hanes, Q. Xu, *Sci. Adv.* **2023**, *9*, adf4608.
[11] X. Liu, Z. Chen, J. Bai, X. Li, X. Chen, Z. Li, H. Pan, S. Li, Q. Gao, N. Zhao, A. Chen, H. Xu, Y. Wen, L. Du, M. Yang, X. Zhou, J. Huang, *ACS Nano* **2023**, *17*, 25377.
[12] L. Zhao, F. Wang, Z. Cai, Q. Zhou, B. Chen, C. Zhang, H. Liu, L. Hong, T. Zhang, J. Zhong, W. Cui, Z. Wang, *Chem. Eng. J.* **2021**, *424*, 130464.
[13] T. Tong, R. Zhao, Y. Yang, W. Shen, X. Yuan, J. Zhang, Y. Yuan, *Nano Today* **2025**, *61*, 102642.
[14] D. Alsoud, B. Verstockt, C. Fiocchi, S. Vermeire, *Lancet Gastroenterol.* **2021**, *6*, 589.
[15] H. Gavilán, S. K. Avugadda, T. Fernández-Cabada, N. Soni, M. Cassani, B. T. Mai, R. Chantrell, T. Pellegrino, *Chem. Soc. Rev.* **2021**, *50*, 11614.
[16] Y. Ma, S. Gou, Z. Zhu, J. Sun, M. Shahbazi, T. Si, C. Xu, J. Ru, X. Sh, R. L. Reis, S. C. Kundu, B. Ke, G. Nie, B. Xiao, *Adv. Mater.* **2024**, *36*, 2309516.
[17] T. Zhang, H. Tian, S. Qin, Y. Gao, X. Zhang, E. C. Nice, Z. Du, C. Huang, *Adv. Funct. Mater.* **2024**, *34*, 2313384.
[18] A. Peairs, R. Dai, L. Gan, S. Shimp, M. N. Rylander, L. Li, C. M. Reilly, *Cell. Mol. Immunol.* **2010**, *7*, 123.
[19] J. Lou, W. Wang, L. Zhu, *Sci. Technol.* **2019**, *53*, 11860.
[20] P. Khiewkamrop, P. Phunsomboon, L. Richert, D. Pekthong, P. Srisawang, *Cancer Cell Int.* **2018**, *18*, 46.
[21] Z. Chen, J. Duan, Y. Diao, Y. Chen, X. Liang, H. Li, Y. Miao, Q. Gao, L. Gui, X. Wang, J. Yang, Y. Li, *Bioact. Mater.* **2021**, *6*, https://doi.org/10.1016/j.bioactmat.2020.07.013.
[22] A. Chiu-Lam, C. Rinaldi, *Adv. Funct. Mater.* **2016**, *26*, 3933.
[23] L. Zhang, Q. Zhang, D. T. Hinojosa, K. Jiang, Q. K. Pham, Z. Xiao, V. L. Colvin, G. Bao, *ACS Nano* **2022**, *16*, 18538, https://doi.org/10.1021/acsnano.2c06776.
[24] J. Xie, J. Xiang, Y. Shen, S. Shao, *Chem. Bio. Eng.* **2025**, *2*, 132.
[25] R. Cheng, L. Jiang, H. Gao, Z. Liu, E. Mäkilä, S. Wang, Q. Saiding, L. Xiang, X. Tang, M. Shi, J. Liu, L. Pang, J. Salonen, J. Hirvonen,

 © 2026 Wiley-VCH GmbH

15214095, 2026, 6, Downloaded from https://advanced.onlinelibrary.wiley.com/doi/10.1002/adma.202514413 by Universidade Do Minho, Wiley Online Library on [21/04/2026]. See the Terms and Conditions (https://onlinelibrary.wiley.com/terms-and-conditions) on Wiley Online Library for rules of use; OA articles are governed by the applicable Creative Commons License

H. Zhang, W. Cui, B. Shen, H. A. Santos, *Adv. Mater.* **2022**, *34*, 2203915.
[26] Y. Wu, S. Wan, S. Yang, H. Hu, C. Zhang, J. Lai, J. Zhou, W. Chen, X. Tang, J. Luo, X. Zhou, L. Yu, L. Wang, A. Wu, Q. Fan, J. Wu, *J. Nanobiotechnol.* **2022**, *20*, 542.
[27] J. Xu, M. Wu, J. Yang, D. Zhao, D. He, Y. Liu, X. Yan, Y. Liu, D. Pu, Q. Tan, L. Zhang, J. Zhang, *Nat. Nanotechnol.* **2024**, *19*, 1544.
[28] Y. Ma, X. Zhang, B. Xuan, D. Li, N. Yin, L. Ning, Y. Zhou, Y. Yan, T. Tong, X. Zhu, X. Huang, M. Hu, Z. Wang, Z. Cui, H. Li, J. Wang, J. Fang, R. Liu, H. Chen, J. Hong, *Gut* **2024**, *73*, 268.
[29] T. R. Nayak, A. Chrastina, J. Valencia, O. Cordova-Robles, R. Yedidsion, T. Buss, B. Cederstrom, J. Koziol, M. D. Levin, B. Olenyuk, J. E. Schnitzer, *Nat. Nanotechnol.* **2025**, *20*, 144.
[30] M. Hering, A. Madi, R. Sandhoff, S. Ma, J. Wu, A. Mieg, K. Richter, K. Mohr, N. Knabe, D. Stichling, G. Poschet, F. Bestvater, L. Frank, J. Utikal, V. Umansky, G. Cui, *Nat. Commun.* **2024**, *15*, 6067.
[31] Y. Lin, X. Yang, W. Yue, X. Xu, B. Li, L. Zou, R. He, *Cell. Mol. Immunol.* **2014**, *11*, 355.
[32] Y. Shen, L. Posavec, S. Bolisetty, F. M. Hilty, G. Nyström, J. Kohlbrecher, M. Hilbe, A. Rossi, J. Baumgartner, M. B. Zimmermann, R. Mezzenga, *Nat. Nanotechnol.* **2017**, *12*, 642.
[33] F. Xiao, Y. Liu, Y. Su, X. He, L. Lu, M. Zhan, L. Wen, Y. Dai, B. Liu, *Chem. Bio. Eng.* **2024**, *1*, 448.
[34] Y. Sun, Y. Zhou, M. Rehman, Y.-F. Wang, S. Guo, *Chem. Bio. Eng.* **2024**, *1*, 757.
[35] K. Gronke, P. P. Hernández, J. Zimmermann, C. S. N. Klose, M. Kofoed-Branzk, F. Guendel, M. Witkowski, C. Tizian, L. Amann, F. Schumacher, H. Glatt, A. Triantafyllopoulou, A. Diefenbach, *Nature* **2019**, *566*, 249.
[36] P. S. Haque, N. Kapur, T. A. Barrett, A. L. Theiss, *Nat. Rev. Gastro. Hepat.* **2024**, *21*, 537.
[37] Q. Huang, Y. Liu, B. R. Dhar, *J. Hazard. Mater.* **2024**, *480*, 135801.
[38] Y. Wang, Q. Zhang, M. Kan, F. Chang, X. He, N. Cheng, K. Huang, *J. Nanobiotechnol.* **2024**, *22*, 524.
[39] R. Le Guern, T. Grandjean, S. Stabler, M. Bauduin, P. Gosset, É. Kipnis, R. Dessein, *Nat. Commun.* **2023**, *14*, 78.
[40] R. Sun, Y. Zhang, X. Zhao, T. Tang, Y. Cao, L. Yang, Y. Tian, Z. Zhang, P. Zhang, F. Xu, *Adv. Sci.* **2025**, *12*, 2412551.
[41] M. Anikisetty, A. G. Gopala Krishna, V. Panneerselvam, A. N. Kamatham, *J. Funct. Foods* **2018**, *40*, 117.
[42] M. A. Frias, A. Hatipoglu, D. A. Foster, *Trends. Endocrin. Met.* **2023**, *34*, 170.
[43] E. Monteagudo-Cascales, V. M. Gumerov, M. Fernández, M. A. Matilla, J. A. Gavira, I. B. Zhulin, T. Krell, *Nat. Commun.* **2024**, *15*, 5867.
[44] J. Zhang, X. Zhang, M. Lu, Y. Chang, Q. Wang, J. Tu, H. Wu, C. Wang, Z. Hong, M. Xiong, L. Song, W. Wei, *Pharmaceuticals* **2023**, *16*, 664.
[45] V. Rothhammer, I. D. Mascanfroni, L. Bunse, M. C. Takenaka, J. E. Kenison, L. Mayo, C. Chao, B. Patel, R. Yan, M. Blain, J. I. Alvarez, H. Kébir, N. Anandasabapathy, G. Izquierdo, S. Jung, N. Obholzer, N. Pochet, C. B. Clish, M. Prinz, A. Prat, J. Antel, F. J. Quintana, *Nat. Med.* **2016**, *22*, 586.
[46] W. Yi, T. S. Kim, *Int. Immunopharmacol.* **2017**, *48*, 146.
[47] J. Liu, Q. Sun, M. Sun, L. Lin, X. Ren, T. Li, Q. Xu, Z. Sun, J. Duan, *Free Radical Bio Med.* **2022**, *181*, 166.
[48] M. Xu, J. Kang, Q. Wang, X. Zuo, Y. Tan, Y. Wei, D. Zhang, L. Zhang, H. Wu, G. Fei, *Resp. Res.* **2024**, *25*, 186.
[49] F. Malard, A. Vekhoff, S. Lapusan, F. Isnard, E. D'incan-Corda, J. Rey, C. Saillard, X. Thomas, S. ucastelle-Lepretre, E. Paubelle, M. Larcher, C. Rocher, C. Recher, S. Tavitian, S. Bertoli, A. Michallet, L. Gilis, P. Peterlin, P. Chevallier, S. Nguyen, E. Plantamura, L. Boucinha, C. Gasc, M. Michallet, J. Dore, O. Legrand, M. Mohty, *Nat. Commun.* **2021**, *12*, 3084.
[50] J. Ouyang, M. Wang, D. Bu, L. Ma, F. Liu, C. Xue, C. Du, A. Aboragah, J. J. Loor, *Front. Nutr.* **2021**, *8*, 760578.
[51] J. Xu, Z. Chen, X. Huang, J. Wu, H. Huang, L. Niu, H. Wang, J. Li, D. B. Lowrie, Z. Hu, S. Lu, X. Fan, *Sci. Adv.* **2024**, *10*, adk8093.
[52] L. Jia, Y. Jiang, L. Wu, J. Fu, J. Du, Z. Luo, L. Guo, J. Xu, Y. Liu, *Nat. Commun.* **2024**, *15*, 1617.
[53] S. W. Wilkinson, A. Hannan Parker, A. Muench, R. S. Wilson, K. Hooshmand, M. A. Henderson, E. K. Moffat, P. S. C. F. Rocha, H. Hipperson, J. H. M. Stassen, A. López Sánchez, I. S. Fomsgaard, P. Krokene, M. H. Mageroy, J. Ton, *Nat. Plants* **2023**, *9*, 81.
[54] L. Liu, F.-M. Sonbol, B. Huot, Y. Gu, J. Withers, M. Mwimba, J. Yao, S. Y. He, X. Dong, *Nat. Commun.* **2016**, *7*, 13099.
[55] N. Kumar, G. Gupta, K. Anilkumar, N. Fatima, R. Karnati, G. V. Reddy, P. V. Giri, P. Reddanna, *Sci. Rep.* **2016**, *6*, 31649.
[56] A. Hu, L. Sun, H. Lin, Y. Liao, H. Yang, Y. Mao, *Signal Transduct. Tar.* **2024**, *9*, 68.
[57] C. Li, Y. Zhao, J. Cheng, J. Guo, Q. Zhang, X. Zhang, J. Ren, F. Wang, J. Huang, H. Hu, R. Wang, J. Zhang, *Adv. Sci.* **2019**, *6*, 1900610.
[58] Q. Nie, C. Li, Y. Wang, Y. Hu, W. Pu, Q. Zhang, J. Cai, Y. Lin, G. Li, C. Wang, L. Li, Y. Dou, J. Zhang, *Acta Pharm. Sin. B* **2023**, *13*, 390.
[59] Q. Zhang, F. Zhang, S. Li, R. Liu, T. Jin, Y. Dou, Z. Zhou, J. Zhang, *Theranostics* **2019**, *9*, 3732.
[60] S. Liu, Y. Cao, L. Ma, J. Sun, L. Ramos-Mucci, Y. Ma, X. Yang, Z. Zhu, J. Zhang, B. Xiao, *J. Control Release* **2022**, *347*, 544.

© 2026 Wiley-VCH GmbH

15214095, 2026, 6, Downloaded from https://advanced.onlinelibrary.wiley.com/doi/10.1002/adma.202514413 by Universidade Do Minho, Wiley Online Library on [21/04/2026]. See the Terms and Conditions (https://onlinelibrary.wiley.com/terms-and-conditions) on Wiley Online Library for rules of use; OA articles are governed by the applicable Creative Commons License